metals

MDPI

Article

Microstructural Changes and Strengthening of Austenitic Stainless Steels during Rolling at 473 K

Marina Odnobokova [1], Andrey Belyakov [2,*], Nariman Enikeev [1,3], Rustam Kaibyshev [2] and Ruslan Z. Valiev [1,3]

1 Institute for Physics of Advanced Materials, Ufa State Aviation Technical University, K. Marx 12, 450008 Ufa, Russia; odnobokova_marina@mail.ru (M.O.); nariman.enikeev@ugatu.su (N.E.); ruslan.valiev@ugatu.su (R.Z.V.)

2 Laboratory of Mechanical Properties of Nanostructured Materials and Superalloys, Belgorod State University, Pobeda 85, 308015 Belgorod, Russia; rustam_kaibyshev@bsu.edu.ru

3 Laboratory of Mechanics of Advanced Bulk Nanomaterials for Innovative Engineering Applications, Saint Petersburg State University, Peterhof, 198504 St. Petersburg, Russia

* Correspondence: belyakov@bsu.edu.ru; Tel.: +7-4722-585-457

Received: 6 November 2020; Accepted: 27 November 2020; Published: 30 November 2020

Abstract: The microstructural changes in 304L and 316L austenitic stainless steels during plate rolling with 95% rolling reduction at a temperature of 473 K and their effect on strengthening were studied. The microstructure evolution was associated with deformation twinning and microshear banding. The latter ones involved ultrafine crystallites, which rapidly evolved in strain-induced ultrafine austenite grains as a result of fast increase in misorientations between them. Besides the ultrafine austenite crystallite evolution, the microshear bands assisted local appearance of deformation martensite, which attained about 25 vol.% and 3 vol.% at total strain of 3 in 304L and 316L steels, respectively. Both the microshear banding and the martensitic transformation promoted the formation of ultrafine grains with a size of less than 1 μm. The strain dependence of the ultrafine grain fraction obeyed a modified Johnson-Mehl-Avrami-Kolmogorov function. The deformation grain size and dislocation density that develop during rolling could also be expressed by exponential functions of true strain. Incorporating the revealed relationships between the strain and the microstructural parameters into modified Hall–Petch-type equation, unique expression for the yield strength of processed steels was obtained. The dislocation strengthening was the largest contributor to the strength, especially at small to medium strains, although grain size strengthening increased during rolling approaching that from dislocations at large strains.

Keywords: austenitic stainless steel; deformation twinning; microshear banding; ultrafine grains; strengthening

1. Introduction

Nowadays, chromium-nickel austenitic stainless steels are widely used in shipbuilding, chemical and petrochemical industries, nuclear industries, medical instruments and implants owing to their good corrosion resistance [1,2]. The most widespread representatives of chromium-nickel austenitic stainless steels are those of 304 and 316 grades. However, the yield strength of solution treated chromium-nickel austenitic steels is relatively low and restricts their usage for structural and engineering applications [3]. Commonly, the structural metals and alloys can be strengthened by the formation of nanocrystalline or ultrafine grained microstructure in course of severe plastic deformation or large strain deformation [4–8]. Among various methods proposed to achieve the large strains, rolling is the most efficient method for production of the sizable semi-products of austenitic stainless steels. A number of researches were

devoted to the deformation microstructure and mechanical properties of austenitic stainless steels (including 304 and 316 series) after cold rolling at room temperature [9–16]. The frequent operation of twinning and martensitic transformation during cold rolling was reported to result in the rapid refinement of the microstructure. As a result of cold rolling to large strains, austenitic stainless steels experienced substantial strengthening; their yield strength could exceed 1500 MPa [10–12,15]. On the other hand, plasticity of these cold worked steels degraded remarkably down to a few percent of tensile elongation. Thus, the cold rolled steel products are frequently annealed to recover plasticity. Desirable compromise between the strength and plasticity was reported after cold rolling followed by fast heat treatment, which released the residual stresses partially but did not coarsen the ultrafine grains remarkably [17–19]. Alternatively, the steel semi-products can be subjected to warm rolling, when dynamic recovery accompanies the evolution of ultrafine grains. Yanushkevich et al. [20] studied the effect of rolling temperature in the range of 773–1173 K on the evolution of the microstructure and the yield strength of 304L—type and 316L—type austenitic stainless steels. The grain refinement was considered in terms of continuous dynamic recrystallization and the maximum value of the yield strength did not exceed 1000 MPa. Further strengthening can be expected after rolling at lower temperatures. However, warm working in the temperature region between 293 K and 773 K remains poorly understood for austenitic stainless steels, although such deformation treatment could provide a desirable combination of strength and ductility. The strengthening of metals and alloys owing to large strain cold or warm deformation is generally discussed in terms of either grain boundary strengthening through the Hall-Petch relationship [21,22], or dislocation strengthening [23,24], or modified Hall-Petch-type relationship including dislocation strengthening [25–27]. It should be noted that both structural parameters, namely, the grain size and the dislocation density, that evolved during cold to warm rolling can be expressed by functions of true strain [15,28,29]. Such approach that could allow expressing the yield strength as a function of true strain seems to be quite beneficial.

The aim of the present study is to quantify the microstructural changes in 304L-type and 316L-type austenitic stainless steels subjected to rolling at 473 K. Particular attentions are paid for the development of strain-induced high-angle grain boundaries, ultrafine crystallites, high dislocation densities, and their contribution to the yield strength.

2. Materials and Methods

Chromium-nickel stainless steels of 304L and 316L type with the chemical compositions shown in Table 1 were selected as starting materials. The original samples were subjected to hot forging at 1373 K to obtain initial blanks with cross section of 30 × 30 mm^2 for subsequent rolling. The initial blanks were plate rolled at a temperature of 473 K to true strains (ε) of 0.5, 1, 2 or 3. The microstructural observations of the rolled samples were performed using electron backscatter diffraction (EBSD) analyser on scanning electron microscope (SEM), Nova Nanosem 450 (FEI, Hillsboro, OR, USA), setting the step sizes of 200 nm, 100 nm and 50 nm for samples rolled to strains of 0.5, 1 and 2–3, respectively. The EBSD data were processed with software of TSL OIM Analysis 6.2 (V6.2, EDAX, Inc., Mahwah, NJ, USA) incorporating an orientation imaging microscopy (OIM) analysis. The fine structure was analyzed using transmission electron microscope (TEM), JEM-2100, (JEOL Ltd., Tokyo, Japan). For EBSD and TEM observations, which were carried out on the ND-RD sample sections (ND and RD are the normal and rolling directions, respectively), the specimens were electro-polished using a solution of 10% perchloric acid ($HClO_4$) in glacial acetic acid ($C_2H_4O_2$). In the OIM micrographs shown in the paper, low-angle subboundaries with misorientations of $2° \leq \theta < 15°$ are indicated by thin black lines, high-angle boundaries with misorientations of $\theta \geq 15°$ are indicated by thick black lines, and twin boundaries are depicted by white lines. The mean grain size was evaluated on the OIM micrographs by a linear intercept method along ND, counting all high-angle austenite, martensite, and interphase boundaries. The dislocation density in (sub)grain interiors was evaluated as a number of dislocations per unit area (counting individual dislocations intersecting arbitrary selected areas on the representative TEM images). The volume fractions of the strain-induced martensite (α') were

averaged through magnetic induction method (Fischer Feritscope FMP30, Helmut Fischer Gmbh, Sindelfingen, Germany), X-ray analysis (Rigaku Ultima IV diffractometer, Rigaku Co., Tokyo, Japan) and EBSD technique. The tensile tests were carried out on Instron 5882 testing machine (ToolWorks Inc., Norwood, MA, USA) at room temperature and crosshead rate of 2 mm/min by using flat specimens with a gauge length of 12 mm and a cross section of 3.0 × 1.5 mm^2 cut with tensile axis along RD.

Table 1. Chemical compositions of the 304L and 316L austenitic stainless steels investigated.

Element[wt.%]	Fe	C	Cr	Ni	Mn	Mo	Si	P	S
304L	Bal.	0.05	18.2	8.8	1.65	0.5	0.43	0.05	0.04
316L	Bal.	0.04	17.3	10.7	1.7	2	0.4	0.04	0.05

3. Results

3.1. Microstructural Evolution

The microstructure evolutions in the 304L and 316L austenitic stainless steels during rolling at a temperature of 473 K are illustrated in Figures 1 and 2, respectively. The main structural parameters of the present steels subjected to rolling at 473 K are summarized in Table 2. Rolling to ε = 0.5 flattens the grains and brings about numerous low-angle subboundaries in both steels. In addition, the deformation is accompanied by the development of deformation twinning that is typical feature of face centered cubic metals with low stacking fault energy (SFE) [30]. The latter is about 20 mJ/m^2 and 25 mJ/m^2 in 304L and 316L steels, respectively [31].

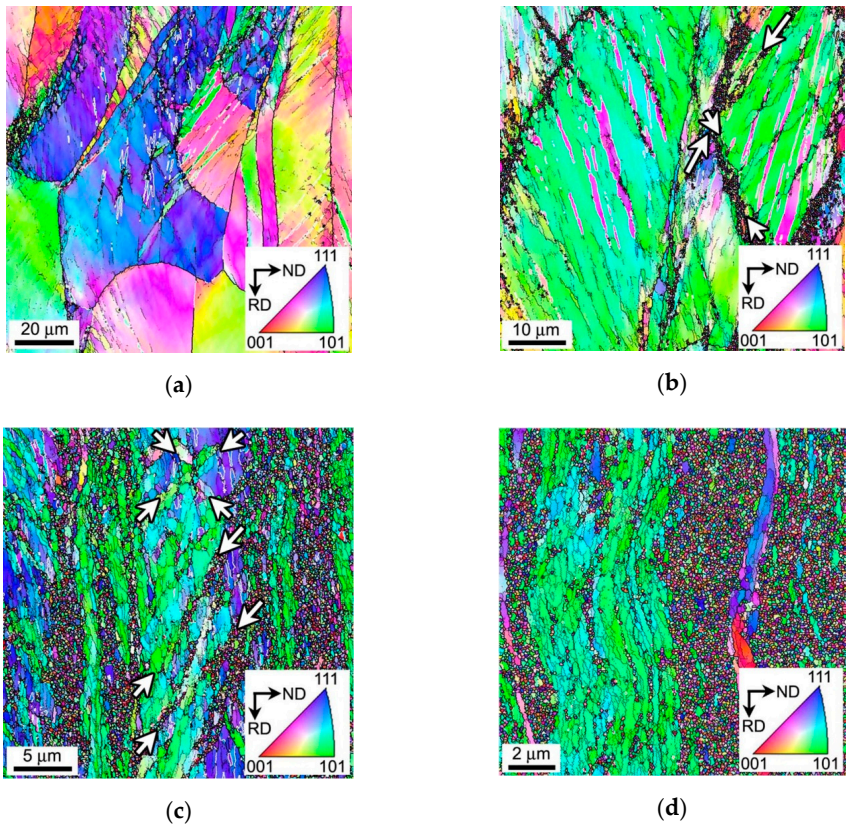

Figure 1. OIM images showing deformation microstructures evolved in a 304L stainless steel during rolling at 473 K to total strains of 0.5 (**a**), 1 (**b**), 2 (**c**) and 3 (**d**). High-angle, low-angle and twin boundaries are indicated by thick black, thin black and white lines, respectively. The inverse pole figures are shown for the normal direction (ND).

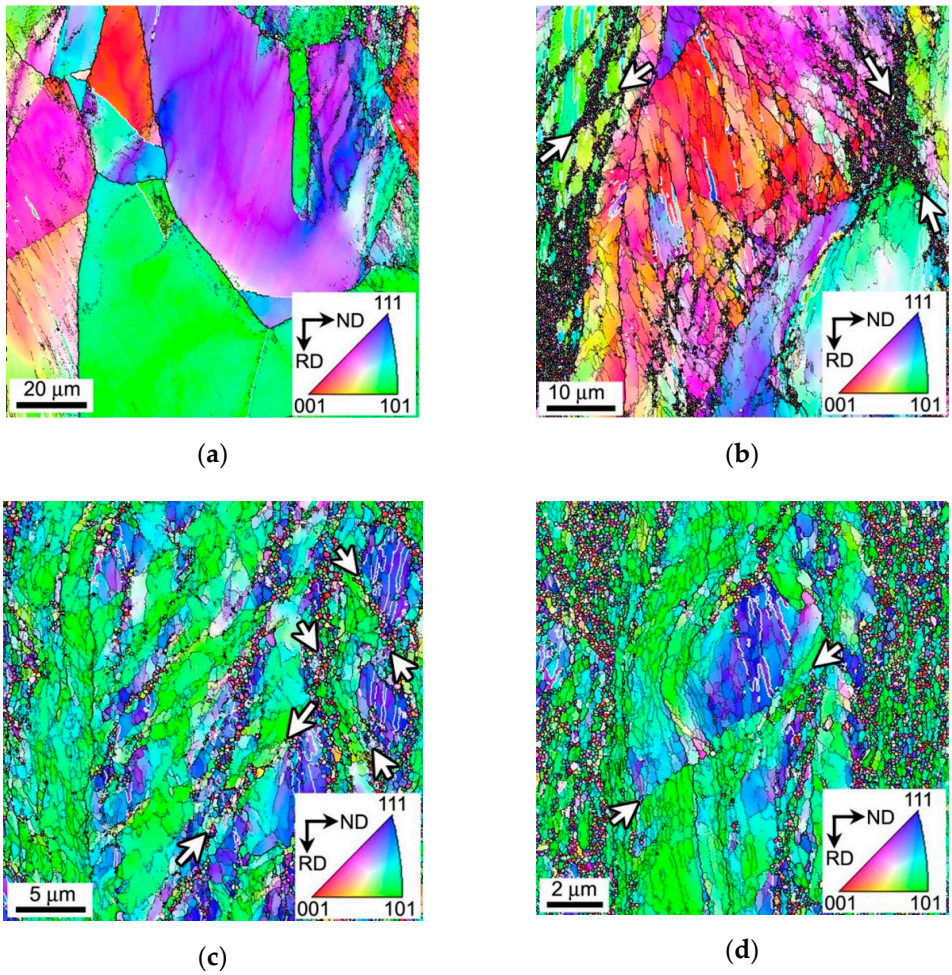

Figure 2. OIM images showing deformation microstructures evolved in a 316L stainless steel during rolling at 473 K to total strains of 0.5 (**a**), 1 (**b**), 2 (**c**) and 3 (**d**). High-angle, low-angle and twin boundaries are indicated by thick black, thin black and white lines, respectively. The inverse pole figures are shown for the normal direction (ND).

Table 2. The grain size (D), the dislocation density (ρ), the martensite fraction (F_M), the yield strength ($\sigma_{0.2}$), the ultimate tensile strength (UTS) and total elongation (δ) of 304L and 316L stainless steels subjected to rolling at 473 K to different strains (ε).

Condition	D, µm	ρ, 10^{15} m^{-2}	F_M, %	$\sigma_{0.2}$, MPa	UTS, MPa	δ, %
Initial (304L)	24 ± 4	0.002 ± 0.001	-	220 ± 20	600 ± 20	100 ± 3
ε = 0.5 (304L)	1.4 ± 0.4	1.8 ± 0.4	0.9 ± 0.7	770 ± 30	800 ± 20	35 ± 3
ε = 1 (304L)	0.5 ± 0.05	2 ± 0.3	2.3 ± 0.9	970 ± 20	1040 ± 20	12 ± 2
ε = 2 (304L)	0.2 ± 0.05	3 ± 0.2	15.3 ± 2.8	1160 ± 10	1250 ± 10	9 ± 2
ε = 3 (304L)	0.13 ± 0.03	3.5 ± 0.2	24.6 ± 2.7	1350 ± 10	1480 ± 10	8 ± 2
Initial (316L)	21 ± 4	0.002 ± 0.001	-	235 ± 20	585 ± 20	86 ± 3
ε = 0.5 (316L)	1.6 ± 0.4	1.4 ± 0.4	0.3 ± 0.3	750 ± 30	790 ± 20	30 ± 3
ε = 1 (316L)	0.55 ± 0.05	1.7 ± 0.3	0.33 ± 0.3	950 ± 20	1030 ± 20	13 ± 2
ε = 2 (316L)	0.25 ± 0.05	2.8 ± 0.2	1.83 ± 0.5	1110 ± 10	1190 ± 10	9 ± 2
ε = 3 (316L)	0.15 ± 0.03	3.4 ± 0.2	2.6 ± 0.3	1240 ± 10	1350 ± 10	9 ± 2

Correspondingly, the number density of twins in 304L steel is higher than that in 316L steel (cf. Figures 1a and 2a). The deformation twinning assists the appearance of the first ultrafine grains with high-angle boundaries, whose misorientations are about 60°. Further rolling to a strain of 1 is accompanied by more frequent development of deformation twinning in both steels. Therefore,

the fraction of twin boundaries in the deformation microstructure remarkably increases (Figures 1b and 2b).

The flattening of initial grains during rolling a 473 K to ε = 1 takes place concurrently with the microshear banding that is aligned at about 40° to RD (some microshear bands are indicated by arrows in Figures 1b and 2b). The development of microshear bands in 304L steel promotes the martensitic transformation. The ultrafine martensite grains readily appear in the microshear bands (Figure 3a). Further rolling to a total strain of 2 leads to an increase in the number of microshear bands, which develop in two directions and intersect each other at an angle of about 90° (Figures 1c and 2c). Intersections of the microshear bands serve as additional nucleation sites for the strain-induced martensite, increasing the martensite fraction in both steels (Figure 3). The deformation microshear banding promotes the formation of strain-induced high-angle grain boundaries. The frequent formation of new high-angle boundaries leads to rapid grain refinement and an increase in the fraction of ultrafine grains. The martensitic transformation also leads to an increase in the fraction of ultrafine grains, because martensite grains appear with a submicrometer size. Thus, the rolled microstructures that evolve at large strain (ε = 3) consist of elongated austenite grains with irregular shapes that are interleaved with nanograined austenite/martensite grains (Figures 1d and 2d). The fine austenite/martensite grains with the transverse size of 130–150 nm are finally formed after rolling to a total strain of 3. It should be noted that 304L steel is characterized by smaller grains and higher dislocation densities as compared to 316L one that is probably associated with more frequent deformation twinning and martensitic transformation.

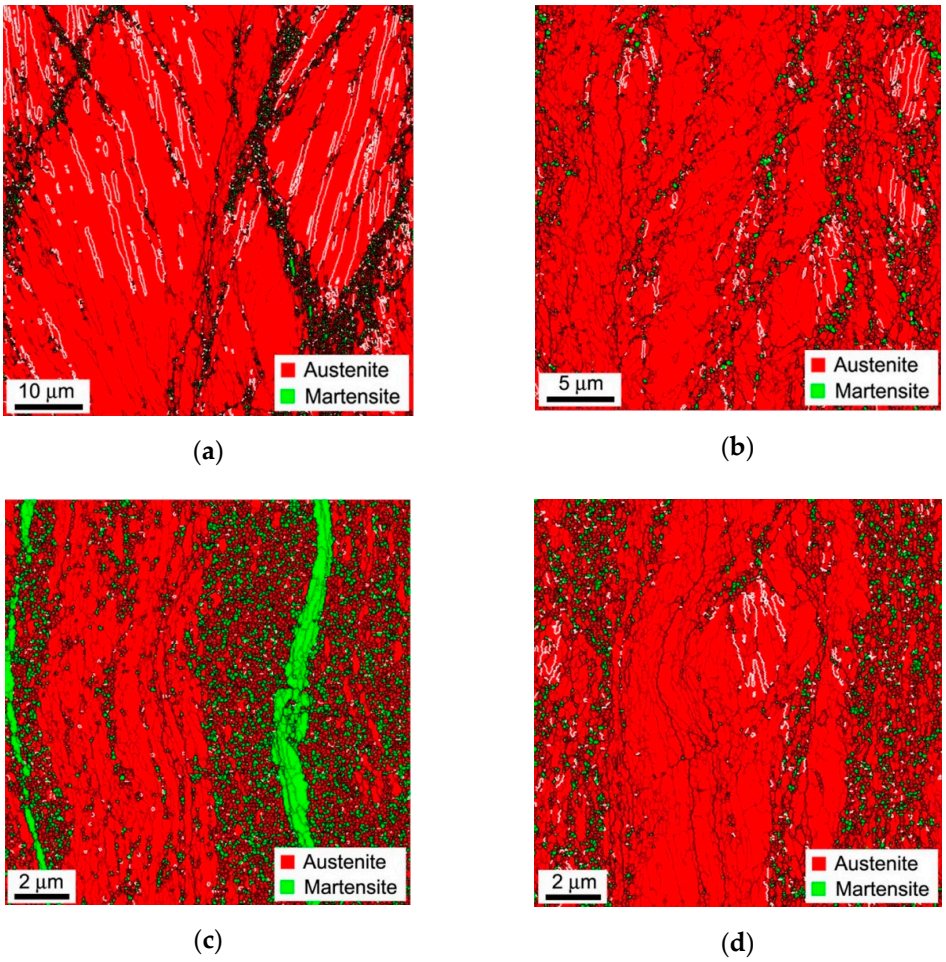

Figure 3. The austenite/martensite phase distribution in 304L (**a**,**c**) and 316L (**b**,**d**) stainless steels during rolling at 473 K to total strains of 1 (**a**), 2 (**b**) and 3 (**c**,**d**). High-angle, low-angle and twin boundaries are indicated by thick black, thin black and white lines, respectively.

The grain refinement in the 304L and 316L steels during rolling at 473 K is illustrated in Figure 4 as the change in the grain size distributions. The latter ones are characterized by one huge peak against large sizes (16 μm to 128 μm in Figure 4) after relatively small strains of 0.5 to 1. An increase in the total strain to 2 results in the progressive formation of ultrafine grains. As a result, the bimodal grain size distributions with two peaks against small (below 1μm) and large (above 8 μm) sizes are developed. The gradual replacement of coarse grains with ultrafine ones leads to an increase in the small size peak to about 0.5 in the grain size distributions after rolling to a total strain of 3. It should be noted that 304L steel exhibits larger fraction of ultrafine grains comparing with 316L steel.

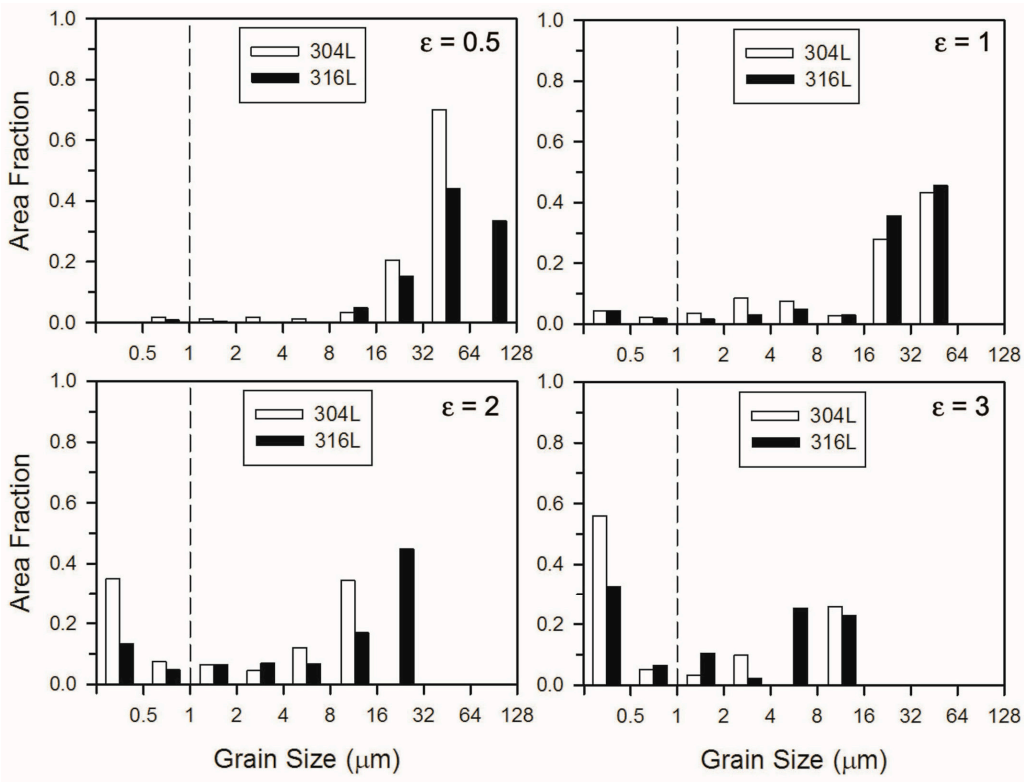

Figure 4. The grain size distributions in 304L and 316L stainless steels subjected to rolling at 473 K to various total strains (ε).

Figure 5 details the twinning, microshear banding and martensite development in the 304L and 316L stainless steel samples during rolling at 473 K. The left-side figures represent the orientation distribution along ND, while the right-side figures show phase maps. The deformation twins are located at 40–60° to ND at a relatively small strain of 0.5 (Figure 5a,b). It is worth noting that a number of deformation subboundaries located almost parallel to twin boundaries can be seen in Figure 5a,b. Thus, the strain-induced subboundaries with low-to-medium misorientations develop nearly parallel to {1 1 1} planes, as suggested by Winter et al. [32]. The deformation twins tend to orient normal to ND with increasing the rolling reduction (Figure 5c,d) that is much similar to other studies on cold rolling of austenitic steels with large reductions [33–35]. In contrast, the microshear bands developed at large rolling strains locate at about 45° to ND in Figure 5c,d. Therefore, the microshear banding at rather large strains is scarcely related to the slip planes. The frequent intersections of the microshear bands composed of ultrafine grains result in the development of so-called "eye" shaped heterogeneous microstructure [36].

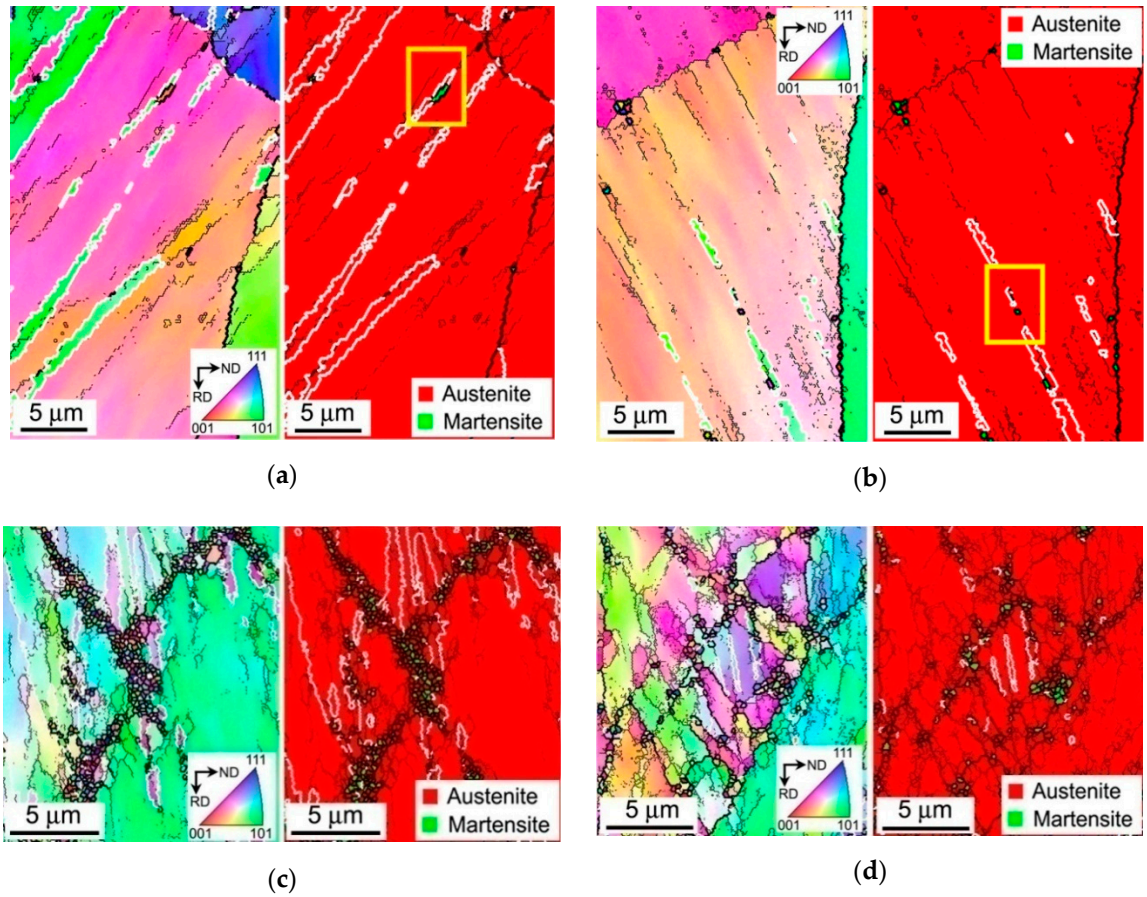

Figure 5. Strain-induced boundaries, twins and martensite in 304L (**a**,**c**) and 316L (**b**,**d**) stainless steels after rolling at 473 K to total strains of 0.5 (**a**,**b**) and 1 (**c**,**d**). High-angle, low-angle and twin boundaries are indicated by thick black, thin black and white lines, respectively.

The nucleation of strain-induced martensite in meta-stable austenitic steels with low SFE frequently takes place at deformation twins [37]. The orientation relationships between austenite and strain-induced martensite are exemplified in Figure 6, which shows the martensite orientation (from the selected portions in Figure 5a,b) as {1 0 0} pole figure corresponding to the orientation of surrounding austenite of {1 1 1}<1 1 2>. The martensite orientations predicted by Bain, Nishiyama-Wassermann (N-W), Kurdjumov–Sachs (K-S) and Pitsch orientation relationships [33] are also indicated in Figure 6. It is clearly seen in Figure 6 that the strain-induced martensite appears close to N–W orientation relationship, although this relationship is obeyed approximately, especially for 316L steel in Figure 6. Remarkable deviation of strain-induced martensite orientation from those predicted by theoretical models has been reported in other studies [38–40].

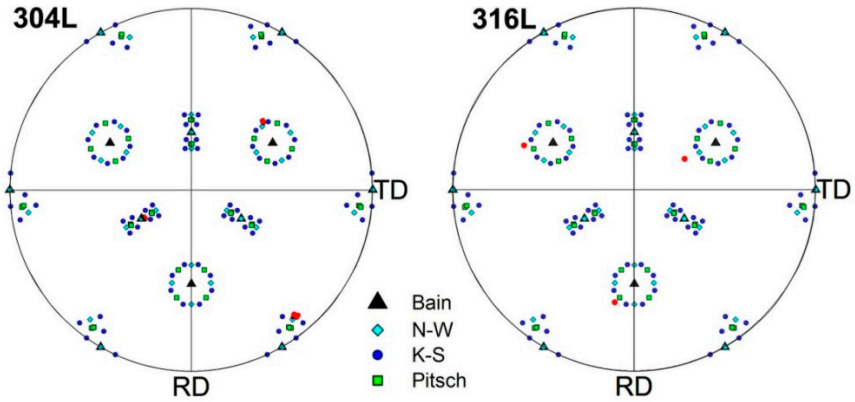

Figure 6. Representative examples of {0 0 1} pole figures of martensite (red points) in 304L and 316L stainless steels, that were obtained from the selected portions in Figure 5a,b, respectively, along with predicted orientations of martensite.

The strain effect on the martensite fraction in the present steels subjected to rolling at 473 K is shown in Figure 7. The martensitic transformation rarely takes place in both steels during rolling to total strains of 0.5 to 1; the martensite fraction does not exceed 3%. The strain-induced martensite rapidly develops in the strain range of $2 < \varepsilon < 3$. The martensite fraction increases to about 25% in the 304L steel with an increase in the rolling strain to 3. It should be noted that the 316L steel is characterized by higher stability against the martensitic transformation, the martensite fraction is not more than 5% after rolling to a total strain of 3. Since the nucleation of martensite occurs heterogeneously within the twins, microshear bands and at their intersections, the strain effect on the martensite fraction in present steels can be described with sigmoid relationship proposed by Olson and Cohen [41]:

$$F_M = 1 - \exp\left(-B(1 - \exp(-A\varepsilon))^m\right), \quad (1)$$

where F_M is the martensite fraction, ε is the total strain, and B, A and m are constants. The values of B, A and m are shown in Figure 7. It should be noted that the dependencies in Figure 7 differ only in the coefficient B, which is greater for 304L steel. Almost the same value of m and much larger values of B and A have been reported for the same steels subjected to rolling at room temperature [15] that reflects slowing down the transformation kinetics with an increase in deformation temperature. Note here that an increase in rolling temperature to 573 K fully suppresses martensitic transformation in these steels [42].

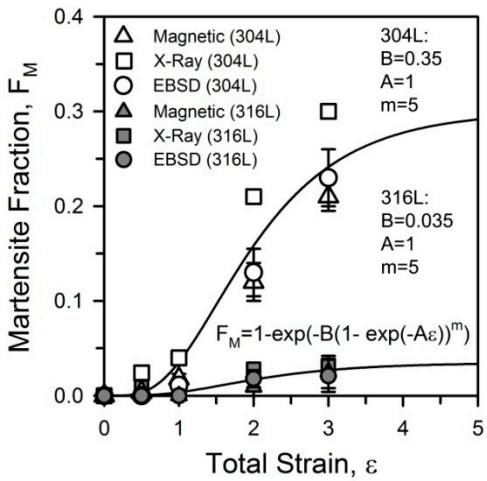

Figure 7. The martensite fraction in 304L and 316L stainless steels subjected to rolling at 473 K to various total strains (ε).

The fine structures that developed in the present steels after rolling at 473 K are represented in Figure 8. Figure 8a,b illustrate the higher density of deformation twins in 304L steel as compared to 316L one. The deformation twins in the fine structure of the present steels look like thin plates with a thickness of about 50 nm. The portions between twins are characterized by dislocation cell substructure with a high dislocation density above 10^{15} m^{-2}. The microshear bands are frequently observed in the 304L and 316L steels after rolling to total strains of 1 and 2, respectively (indicated as MSB in Figure 8c,d). The microshear bands consist of ultrafine austenite and martensite crystallites with a thickness of 50 to 100 nm. An increase in the total strain to 3 leads to the formation of ultrafine grains with a high dislocation density (Figure 8e,f). The Debye-Scherrer rings typical of ultrafine crystalline structures are observed (s. the selected area electron diffraction patterns in Figure 8e,f). It is worth noting that the rings from martensite on the electron diffraction pattern of 304L steel are more pronounced than those of 316L steel, confirming the faster kinetics of martensitic transformation in 304L steel.

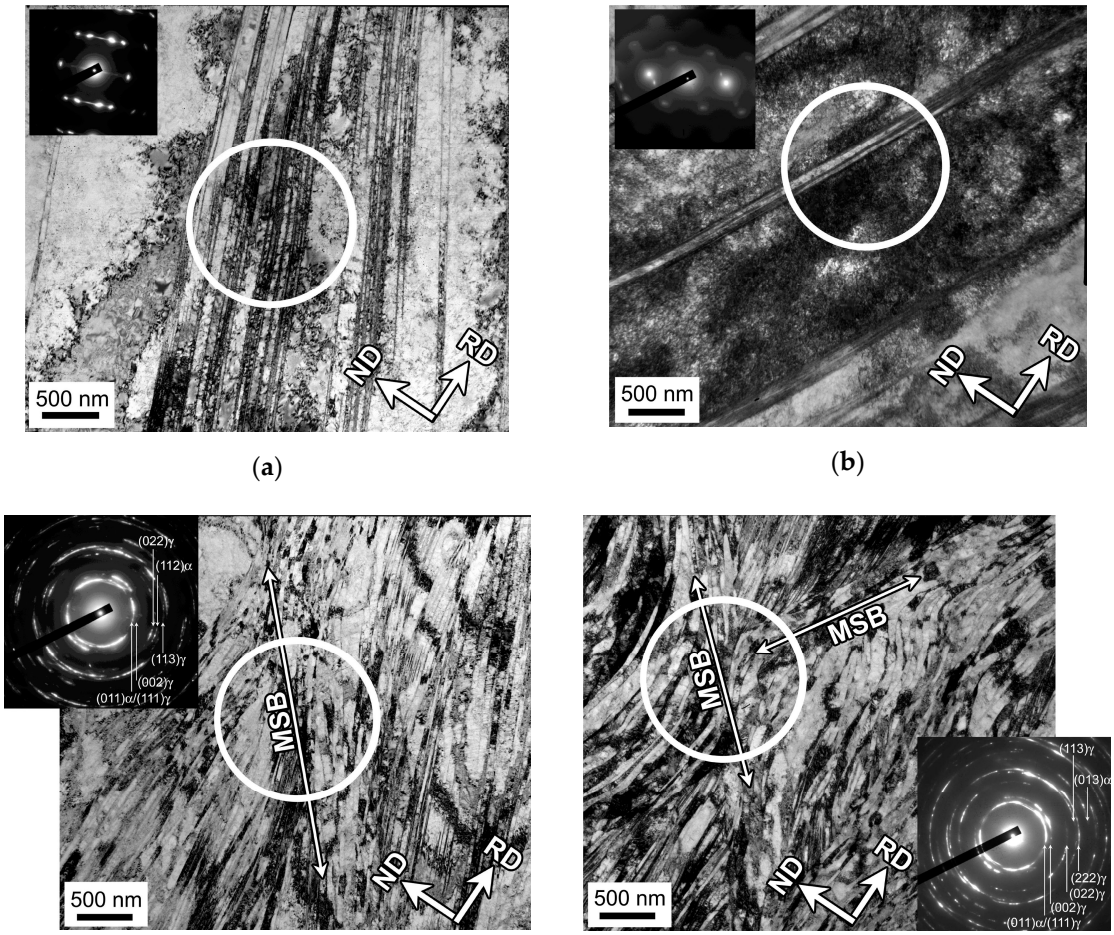

Figure 8. *Cont.*

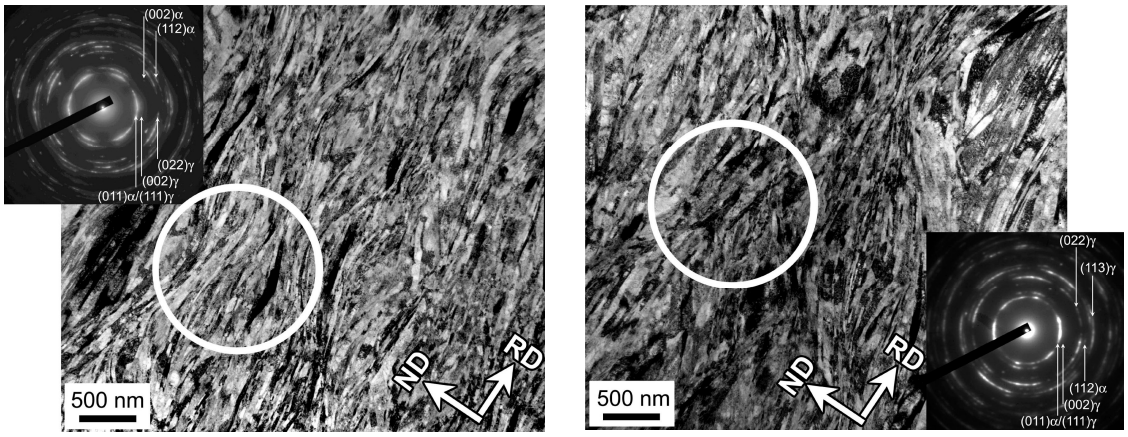

(**e**) (**f**)

Figure 8. Fine structures in 304L (**a**,**c**,**e**) and 316L (**b**,**d**,**f**) stainless steels subjected to rolling at 473 K to total strains of 0.5 (**a**,**b**), 1 (**c**), 2 (**d**) and 3 (**e**,**f**). The circles indicate the portions for selected area electron diffraction patterns.

The mechanisms of microstructure evolution in the stainless steels during rolling at 473 K are clearly reflected on the (sub)grain boundary misorientation distributions that have evolved at different strain levels (Figure 9). The misorientation distributions after relatively small strains are characterized by two sharp peaks at small angles below 15° and large angles about 60° in both steels. Evidently, the first peak corresponds to numerous deformation subboundaries, whereas the second one is associated with the strain-induced twin boundaries. An increase in the misorientation of strain-induced (sub)boundaries leads to a gradual decrease in the fraction of low-angle subboundaries with straining. On the other hand, the fraction of twin boundaries increases to its maximum during rolling to a strain of 1 followed by a decrease with further straining. Somewhat larger fraction of twin boundaries in 304L steel as compared to 316L one is attributed to lower SFE and, as a result, more frequent twinning in the former. Progressive development of the strain-induced high-angle grain boundaries during rolling to large total strains leads to the wide angular distribution of misorientations with a small peak at about 45° similar to random misorientation distribution [43]. Pronounced twinning and martensitic transformation in 304L steel are responsible to larger fraction of randomly misoriented grain boundaries as compared to 316L steel.

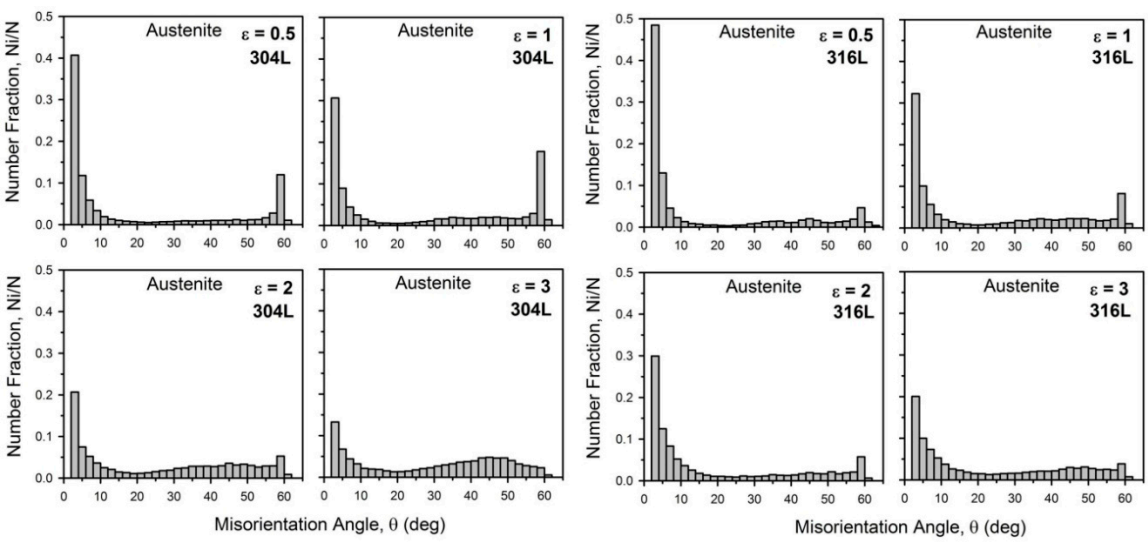

Figure 9. (Sub)grain boundary misorientation distributions evolved in austenite of 304L and 316L stainless steels subjected to rolling at 473 K to various total strains (ε).

3.2. Tensile Behavior

The stress-elongation curves obtained by tensile tests of the 304L and 316L stainless steels after rolling at 473 K to various true strains (ε) are shown in Figure 10. Some tensile properties of the present steels subjected to rolling at 473 K are listed in Table 2. After rolling to strains of 0.5 and 1, the present steels are characterized by similar tensile curves with close values of yield strength, i.e., 750–770 MPa after ε = 0.5 and 950–970 MPa after ε = 1, and elongation, i.e., 30–35% after ε = 0.5 and 12–13% after ε = 1. It is worth noting that both steels processed by rolling to a strain of 0.5 exhibit pronounced stage of uniform elongation without remarkable strain hardening. Such behavior may be attributed to superposition of preliminary work hardening by warm rolling, which increases the yield strength on the inherent ability of austenitic stainless steels to strain hardening that suppresses the necking upon subsequent tensile tests, although this interesting phenomenon deserves further investigation.

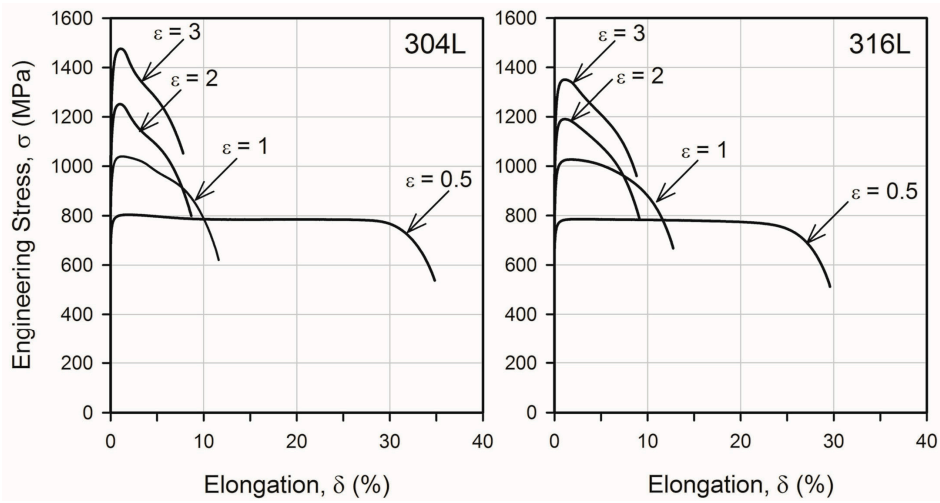

Figure 10. Engineering stress—elongation curves for 304L and 316L stainless steels subjected to rolling at 473 K to various total strains (ε) and then tensile tested at room temperature and at a crosshead rate of 2 mm/min.

Total elongation of both steels decreases to 8–9% after rolling to strains of 2–3. In contrast to ductility, the tensile strength increases greatly with an increase in total strain from 2 to 3. The yield strength increases from 1160 MPa to 1350 MPa in 304L steel, and from 1110 MPa to 1240 MPa in 316L steel after straining from 2 to 3. The 304L steel samples exhibit higher strength as compared to the 316L steel samples after large rolling reductions, although the initial samples exhibited the same strength. This suggests that the 304L steel with lower SFE is more susceptible to grain refinement and work hardening than 316L one during both rolling at 473 K and subsequent tensile tests. Nevertheless, both steels exhibit high yield strength well above 1000 MPa after large strain rolling at 473 K, although limited plasticity (few percent of uniform elongation) may require an additional recovery annealing for certain structural applications.

4. Discussion

4.1. Grain Refinement

Based on structural studies, the sequence of microstructural changes that are associated with to the development of ultrafine grains in 304L and 316L stainless steels during rolling at 473 K with large reduction is represented in Figure 11. Numerous deformation twins and low-angle subboundaries evolve at small strains following rapid increase in dislocation density at early deformation. An increase in strain is accompanied with an increase in misorientations of strain-induced subboundaries, leading to the development of new grain boundaries of deformation origin. Then, the number of such

strain-induced boundaries progressively increases, owing to frequent microshear banding and partial martensitic transformation during further straining. At rather large total strains, new ultrafine grains develop at microshear bands as well as in other portions of microstructural inhomogeneity such as vicinities of original and deformation grain boundaries and their junctions.

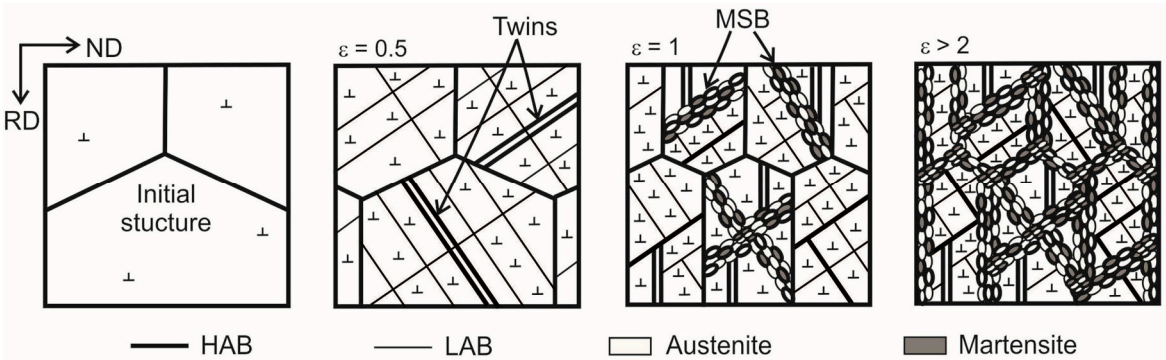

Figure 11. Schematic representation of the structural changes in austenitic stainless steels during rolling at 473 K. MSB—microshear bands, HAB—high-angle boundaries and LAB—low-angle boundaries.

The formation of new ultrafine austenite grains during rolling at 473 K occurs heterogeneously as a result of strain localization in deformation twins and microshear bands. The nucleation of ultrafine martensite grains readily takes place within the microshear bands and their intersections that are also distributed heterogeneously. Thus, the grain refinement kinetics in the present steels during rolling at 473 K is similar to that in the case of discontinuous dynamic recrystallization, which frequently accompanies hot deformation of austenite steels and can be described using a simplified modification of the Johnson–Mehl–Avrami–Kolmogorov equation [44–46]:

$$F_{UFG} = 1 - \exp(-k\varepsilon^n), \tag{2}$$

where F_{UFG} is the fraction of ultrafine grains, k and n are constants.

In this study, F_{UFG} was taken as the area fraction of grains with a size below 1 μm (in Figure 4). The grain refinement kinetics in the 304L and 316L steels during rolling at 473 K are represented in Figure 12, which shows the ultrafine grain fractions as function of rolling strain. The measured ultrafine grain fractions are indicated by symbols in Figure 12, whereas those approximated by Equation (2) are shown by solid lines.

The fraction of ultrafine grains follows sigmoid function of total rolling strain that reflects gradual formation of new ultrafine grains. The formation of new grains is mainly associated with the intersection of deformation twinning and microshear banding. Thus, a decrease in the mean grain size results from increasing the number of ultrafine grains with a size of D_{UFG}. Therefore, the mean austenite/martensite grain size (D_ε) in the present steels during rolling at 473 K can be expressed as follows [15,28]:

$$D_\varepsilon = D_{UFG}(F_{UFG})^{-0.5} = D_{UFG}(1 - \exp(-k\varepsilon^n))^{-0.5}, \tag{3}$$

where D_{UFG} = 100 nm can be taken, since the ultrafine grain size tends to approach 100 nm in large strains.

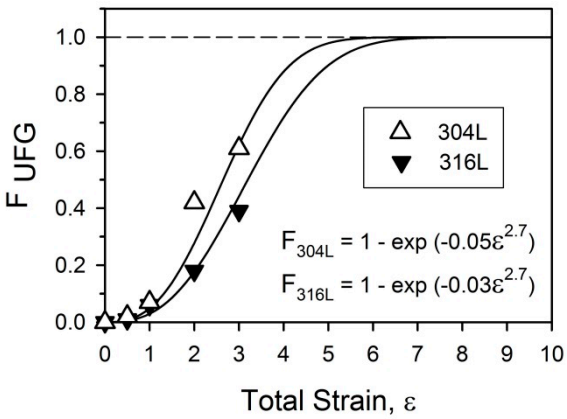

Figure 12. The effect of rolling at 473 K on the fraction of ultrafine grains (F_{UFG}) in 304L and 316L stainless steels.

The changes in the mean grain size in 304L and 316L steels during rolling at 473 K are represented in Figure 13, where the experimentally measured austenite/martensite grain sizes are indicated by symbols and the mean grain sizes calculated by Equation (3) are shown by solid lines. Note here that the values of k and n for Equation (3) are shown in Figure 12. It is seen in Figure 13 that the mean grain sizes calculated by Equation (3) match the experimental values well. A similar approach to predict the grain evolution during deformation has provided a good agreement between the experiment and calculation for austenitic stainless steels, which were cold rolled at room temperature [15]. Somewhat larger k and smaller n obtained for rolling at ambient temperature [15] correspond to more rapid grain refinement because of intensive deformation twinning, microshearing and martensitic transformation at lower temperature. Thus, the assumption based on Equations (2) and (3) can be used to predict the deformation microstructures in austenitic stainless steels in a wide range of rolling conditions.

The dislocation density in present steels continuously increases during rolling at 473 K. According to the Mecking–Kocks theory, the change in the dislocation density during plastic deformation results from competition between athermal hardening (ρ_ε) and dynamic recovery ($R_v \rho$) [23]:

$$\frac{d\rho}{d\varepsilon} = \rho_\varepsilon - R_v\, \rho\,, \tag{4}$$

which can be fairly accurately represented by an exponential function of true strain [29,42]. The results of such representation are shown by solid lines in Figure 14, where the measured values of dislocation density in austenite/martensite crystallites are indicated by triangle symbols.

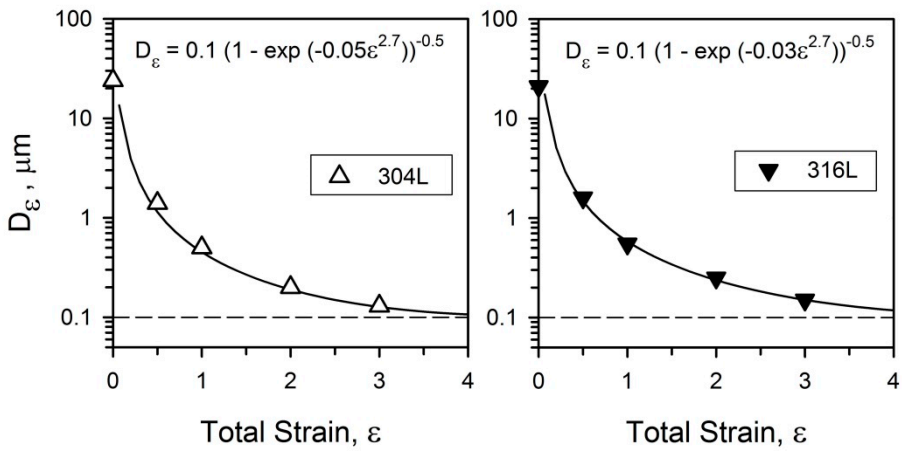

Figure 13. The effect of rolling at 473 K on the mean grain size (D_ε) in 304L and 316L stainless steels.

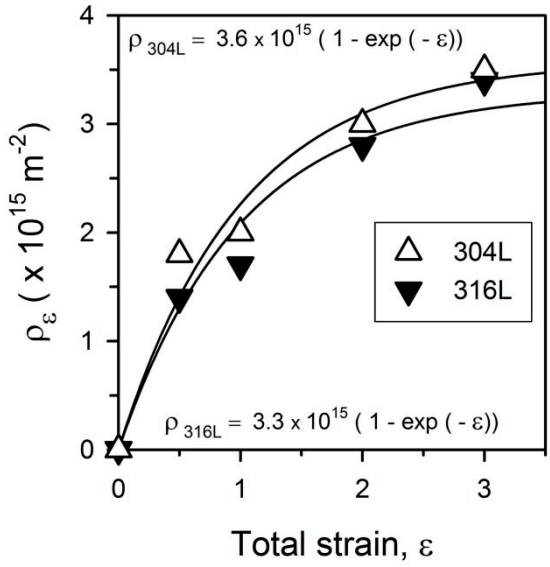

Figure 14. The effect of rolling at 473 K on the dislocation density (ρ_ε) in 304L and 316L stainless steels.

4.2. Strengthening Mechanisms

Rolling at 473 K leads to substantial grain refinement assisted by the development of mechanical twinning and microshear banding that are accompanied by an increase in dislocation density. The latter has been frequently considered as the main strengthening contributor during cold deformation [23,24] irrespective of some changes in grain boundary assemblies [47]. It should be noted that the strengthening of high-Mn austenitic twinning induced plasticity (TWIP)/transformation induced plasticity (TRIP) steels has been also discussed in terms of dislocation strengthening as a result of decreasing the dislocation mean free path because of frequent deformation twins and martensite plates [48]. On the other hand, the development of ultrafine grains during severe plastic deformation has been shown accompanying with an apparent decrease in the dislocation density in their interiors, while internal (residual) stresses have correspondingly increased gradually approaching saturation at large strains [49]. Thus, using the dislocation density as single structural parameter to evaluate the strength of the present warm rolled steels with complicated deformation microstructures seems to be oversimplified. Good agreement between actual and predicted yield strength ($\sigma_{0.2}$) has been obtained by modification of the Hall–Petch relationship, incorporating substructural strengthening aroused by high dislocation density (ρ_ε) in addition to grain boundary strengthening expressed by the mean deformation grain size (D_ε) [50,51]:

$$\sigma_{0.2} = \sigma_0 + K_\varepsilon D_\varepsilon^{-0.5} + \alpha M G b \rho_\varepsilon^{0.5}, \quad (5)$$

where σ_0 is the yield stress of dislocation-free steel with infinite grain size, G is the shear modulus, b is the Burger vector, M is the Taylor factor ($M \approx 3$ for fcc alloys), K_ε and α are constants. The mean grain size (D_ε) and dislocation density (ρ_ε) after rolling at 473 K can be expressed by exponential functions of true strain (s. Figures 13 and 14). Then, the yield strength dependence on the grain size and the dislocation density can be approximated by a plane as shown in Figure 15, using calculated D_ε and ρ_ε from Figures 13 and 14, and taking $G = 81 \times 10^3$ MPa, b = 0.25 nm, σ_0 = 200 MPa, K_ε = 160 MPa × $\mu m^{-0.5}$ and α = 0.19 for the present steel samples. Note here that the value of σ_0 coincides with that obtained by Young and Sherby [52] for stainless steels, the values of K_ε and α are close to those reported by Yanushkevich at al. [27] for austenitic stainless steel subjected to rolling in a wide deformation conditions. Probably, a relatively small amount of martensite does not significantly affect K_ε in the present steel samples. Moreover, the same grain boundary strengthening factors for austenite and strain-induced martensite have been suggested in previous study on the strengthening of 304-type stainless steel subjected to cold rolling [11].

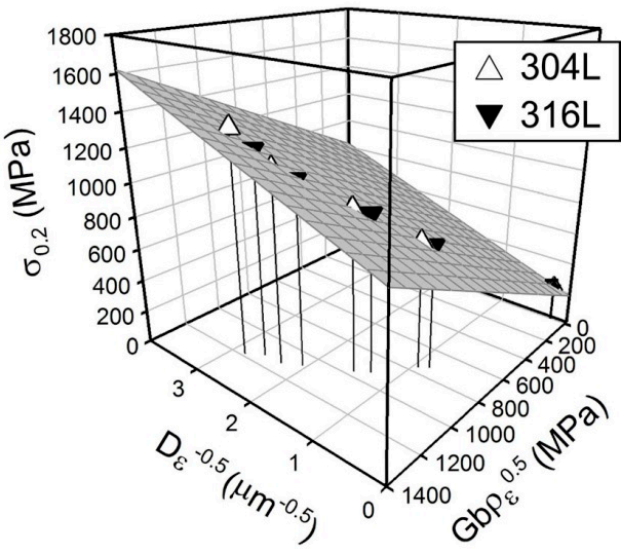

Figure 15. Relationship between the yield strength ($\sigma_{0.2}$), the grain size (D_ε) and dislocation density (ρ_ε) strengthening in 304L and 316L stainless steels subjected to rolling at 473 K.

Using the relationships of D_ε—ε (Figure 13) and ρ_ε—ε (Figure 14), the modified Hall–Petch relationship (Equation (5)) can be written in the following form:

$$\sigma_{0.2} = \sigma_0 + K_\varepsilon \left(D_{UFG}\left(1 - \exp\left(-k\varepsilon^n\right)\right)^{-0.5}\right)^{-0.5} + \alpha MGb\left(\beta\left(1 - \exp(-\varepsilon)\right)\right)^{0.5}. \quad (6)$$

The strain effect on the yield strength and variation of the strengthening contributors in accordance with Equation (6) are shown in Figure 16. The dislocation strengthening provides the main contribution to the strength. The fast increase in the dislocation density above 10^{15} m^{-2} after rolling to a strain of 0.5 provides the strength increment of 400–450 MPa, while the grain size contribution amounts to 120–140 MPa. An increase in the total strain leads to a decrease in the difference between the grain size and dislocation strengthening, although the dislocation strengthening prevails over the grain size strengthening. Clear correlation of the experimental and calculated yield strength in Figure 16 confirms the reliability of proposed approach, which can be used to predict the strength of austenitic stainless steels subjected to warm rolling.

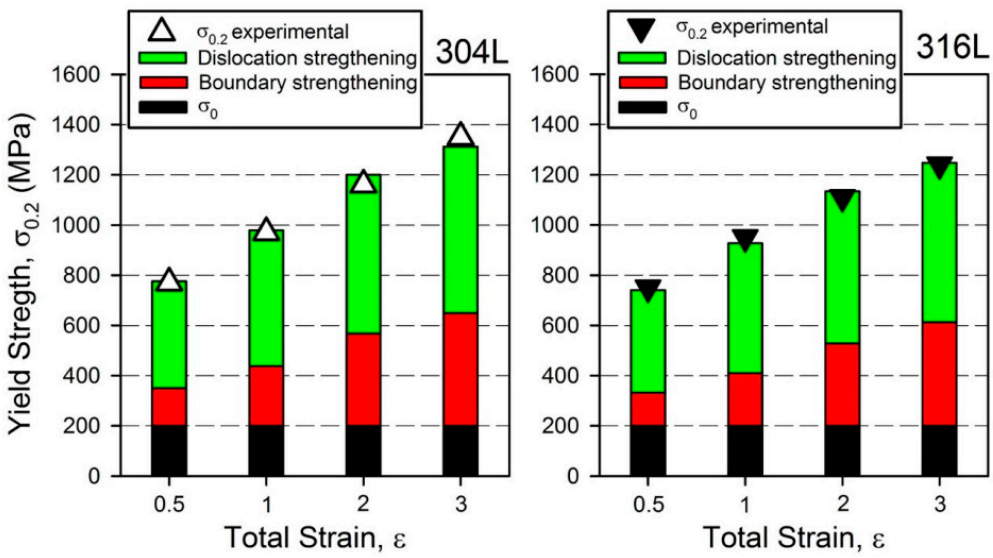

Figure 16. Contribution of different strengthening mechanisms to general yield strength of 304L and 316L stainless steels subjected to rolling at 473 K.

5. Conclusions

The development of ultrafine grained microstructures and mechanical properties of 304L and 316L austenitic stainless steels subjected to large strain rolling at 473 K were studied. The main results can be summarized as follows:

1. Rolling is accompanied by the concurrent operation of deformation twinning, microshear banding and partial martensitic transformation with different kinetics. The 316L steel is more stable against martensitic transformation than 304L steel. The martensite fractions comprise 0.25 in the 304L steel and only 0.03 in the 316L steel after rolling to a total strain of 3.
2. Large strain rolling leads to the development of ultrafine grains, which evolve heterogeneously in the microstructural portions with high density of mutually crossed deformation twins, microshear bands, and martensite lamellas. The strain dependence of the fraction of ultrafine grains (F_{UFG}) can be expressed by a modified Johnson-Mehl-Avrami-Kolmogorov equation as $F_{UFG} = 1 - \exp(-k\varepsilon^{n*})$, where k and n* are constants. In turn, the mean grain size (D_ε) can be expressed as $D_\varepsilon = D_{UFG} (F_{UFG})^{-0.5}$, where D_{UFG} can be taken as a final minimal size of ultrafine grains.
3. The development of ultrafine grained microstructures with high dislocation density during rolling at 473 K results in significant strengthening. The yield strength increased from 220–230 MPa in the original annealed state to 1350 and 1240 MPa in 304L and 316L steels after rolling to a total strain of 3, respectively. The yield strength ($\sigma_{0.2}$) can be expressed by modified Hall-Petch type relationship including the grain size and dislocation strength contributors, which can be expressed through true total strain. The dislocation strengthening provides the main contribution to the yield strength, although the difference between the grain size and dislocation density strengthening decreases with an increase in total strain.

Author Contributions: Conceptualization, A.B. and M.O.; methodology, R.K. and R.Z.V.; formal analysis, N.E.; investigation, M.O.; writing—original draft preparation, A.B. and M.O.; writing—review and editing, N.E., R.K. and R.Z.V. All authors have read and agreed to the published version of the manuscript.

Funding: The reported study was funded by Russian Foundation for Basic Research, RFBR, project number 19-38-60047, covering the microstructural investigations and the mechanical property analysis. Ruslan Z. Valiev acknowledges the support from the Ministry of Science and Higher Education of the Russian Federation, agreement No. 0838-2020-0006, in part of modeling the austenite-martensite orientation relationship.

Conflicts of Interest: The authors declare no conflict of interest.

References

1. Lo, K.H.; Shek, C.H.; Lai, J.K.L. Recent developments in stainless steels. *Mater. Sci. Eng. R Rep.* **2009**, *65*, 39–104. [CrossRef]
2. Venkatsurya, P.; Thein-Han, W.; Misra, R.; Somani, M.; Karjalainen, L. Advancing nanograined/ultrafine-grained structures for metal implant technology: Interplay between grooving of nano/ultrafine grains and cellular response. *Mater. Sci. Eng. C* **2010**, *30*, 1050–1059. [CrossRef]
3. Martienssen, W.; Warlimont, H. *Springer Handbook of Condensed Matter and Materials Data*; Springer: Berlin, Germany, 2005.
4. Valiev, R.Z.; Islamgaliev, R.K.; Alexandrov, I.V. Bulk nanostructured materials from severe plastic deformation. *Prog. Mater. Sci.* **2000**, *45*, 103–189. [CrossRef]
5. Valiev, R. Nanostructuring of metals by severe plastic deformation for advanced properties. *Nat. Mater.* **2004**, *3*, 511–516. [CrossRef] [PubMed]
6. Estrin, Y.; Vinogradov, A. Extreme grain refinement by severe plastic deformation: A wealth of challenging science. *Acta Mater.* **2013**, *61*, 782–817. [CrossRef]
7. Valiev, R.Z.; Zhilyaev, A.P.; Langdon, T.G. *Bulk Nanostructured Materials: Fundamentals and Applications*; John Wiley & Sons: Hoboken, NJ, USA, 2013.
8. Sabirov, I.; Enikeev, N.; Murashkin, M.Y.; Valiev, R.Z. *Bulk Nanostructured Materials with Multifunctional Properties*; Springer: Berlin, Germany, 2015.

9. Belyakov, A.; Odnobokova, M.; Kipelova, A.; Tsuzaki, K.; Kaibyshev, R. Nanocrystalline structures and tensile properties of stainless steels processed by severe plastic deformation. *IOP Conf. Ser. Mater. Sci. Eng.* **2014**, *63*, 012156. [CrossRef]
10. Odnobokova, M.; Belyakov, A.; Kaibyshev, R. Effect of Severe Cold or Warm Deformation on Microstructure Evolution and Tensile Behavior of a 316L Stainless Steel. *Adv. Eng. Mater.* **2015**, *17*, 1812–1820. [CrossRef]
11. Odnobokova, M.; Belyakov, A.; Kaibyshev, R. Development of Nanocrystalline 304L Stainless Steel by Large Strain Cold Working. *Metals* **2015**, *5*, 656–668. [CrossRef]
12. Shakhova, I.; Belyakov, A.; Yanushkevich, Z.; Tsuzaki, K.; Kaibyshev, R. On Strengthening of Austenitic Stainless Steel by Large Strain Cold Working. *ISIJ Int.* **2016**, *56*, 1289–1296. [CrossRef]
13. Li, J.; Gao, B.; Huang, Z.; Zhou, H.; Mao, Q.; Li, Y. Design for strength-ductility synergy of 316L stainless steel with heterogeneous lamella structure through medium cold rolling and annealing. *Vacuum* **2018**, *157*, 128–135. [CrossRef]
14. Sun, G.; Du, L.; Hu, J.; Zhang, B.; Misra, R. On the influence of deformation mechanism during cold and warm rolling on annealing behavior of a 304 stainless steel. *Mater. Sci. Eng. A* **2019**, *746*, 341–355. [CrossRef]
15. Odnobokova, M.; Belyakov, A.; Kaibyshev, R. Grain refinement and strengthening of austenitic stainless steels during large strain cold rolling. *Philos. Mag.* **2019**, *99*, 531–556. [CrossRef]
16. Sohrabi, M.J.; Mirzadeh, H.; Dehghanian, C. Significance of Martensite Reversion and Austenite Stability to the Mechanical Properties and Transformation-Induced Plasticity Effect of Austenitic Stainless Steels. *J. Mater. Eng. Perform.* **2020**, *29*, 3233–3242. [CrossRef]
17. Lei, C.; Li, X.; Deng, X.; Wang, Z. Microstructural Evolution and Microstructure–Mechanical Property Correlation in Nano/ultrafine-Grained Fe-17Cr-6Ni Austenitic Steel. *Metall. Mater. Trans. A* **2018**, *49*, 6134–6146. [CrossRef]
18. Kumar, B.R.; Sharma, S.; Mahato, B. Formation of ultrafine grained microstructure in the austenitic stainless steel and its impact on tensile properties. *Mater. Sci. Eng. A* **2011**, *528*, 2209–2216. [CrossRef]
19. Odnobokova, M.; Yanushkevich, Z.; Kaibyshev, R.; Belyakov, A. On the Strength of a 316L-Type Stainless Steel Subjected to Cold or Warm Rolling Followed by Annealing. *Materials* **2020**, *13*, 2116. [CrossRef]
20. Yanushkevich, Z.; Dobatkin, S.V.; Belyakov, A.; Kaibyshev, R. Hall-Petch relationship for austenitic stainless steels processed by large strain warm rolling. *Acta Mater.* **2017**, *136*, 39–48. [CrossRef]
21. Hall, E. The deformation and ageing of mild steel: II characteristics of the Lüders deformation. *Proc. Phys. Soc. Sect. B* **1951**, *64*, 742. [CrossRef]
22. Petch, N. The cleavage strength of polycrystals. *J. Iron Steel Inst.* **1953**, *174*, 25–28.
23. Mecking, H.; Kocks, U. Kinetics of flow and strain-hardening. *Acta Metall.* **1981**, *29*, 1865–1875. [CrossRef]
24. Estrin, Y.; Toth, L.; Molinari, A.; Bréchet, Y. A dislocation-based model for all hardening stages in large strain deformation. *Acta Mater.* **1998**, *46*, 5509–5522. [CrossRef]
25. Hughes, D.A.; Hansen, N. Microstructure and strength of nickel at large strains. *Acta Mater.* **2000**, *48*, 2985–3004. [CrossRef]
26. Hansen, N. Hall-Petch relation and boundary strengthening. *Scr. Mater.* **2004**, *51*, 801–806. [CrossRef]
27. Yanushkevich, Z.; Mogucheva, A.; Tikhonova, M.; Belyakov, A.; Kaibyshev, R. Structural strengthening of an austenitic stainless steel subjected to warm-to-hot working. *Mater. Charact.* **2011**, *62*, 432–437. [CrossRef]
28. Morozova, A.; Kaibyshev, R. Grain refinement and strengthening of a Cu–0.1Cr–0.06Zr alloy subjected to equal channel angular pressing. *Philos. Mag.* **2017**, *97*, 2053–2076. [CrossRef]
29. Kusakin, P.; Belyakov, A.; Kaibyshev, R.; Molodov, D. Modeling the effect of deformation on strength of a Fe-23Mn-0.3 C-1.5 Al TWIP steel. *IOP Conf. Ser. Mater. Sci. Eng.* **2014**, *63*, 012059. [CrossRef]
30. Schramm, R.E.; Reed, R.P. Stacking fault energies of seven commercial austenitic stainless steels. *Metall. Trans. A* **1975**, *6*, 1345–1351. [CrossRef]
31. De Bellefon, G.M.; van Duysen, J.; Sridharan, K. Composition-dependence of stacking fault energy in austenitic stainless steels through linear regression with random intercepts. *J. Nucl. Mater.* **2017**, *492*, 227–230. [CrossRef]
32. Winther, G.; Huang, X.; Godfrey, A.; Hansen, N. Critical comparison of dislocation boundary alignment studied by TEM and EBSD: Technical issues and theoretical consequences. *Acta Mater.* **2004**, *52*, 4437–4446. [CrossRef]
33. Lü, Y.; Molodov, D.A.; Gottstein, G. Correlation between microstructure and texture development in a cold-rolled TWIP steel. *ISIJ Int.* **2011**, *51*, 812–817. [CrossRef]

34. Kusakin, P.; Belyakov, A.; Haase, C.; Kaibyshev, R.; Molodov, D.A. Microstructure evolution and strengthening mechanisms of Fe–23Mn–0.3 C–1.5 Al TWIP steel during cold rolling. *Mater. Sci. Eng. A* **2014**, *617*, 52–60. [CrossRef]
35. Yanushkevich, Z.; Belyakov, A.; Haase, C.; Molodov, D.A.; Kaibyshev, R. Structural/textural changes and strengthening of an advanced high-Mn steel subjected to cold rolling. *Mater. Sci. Eng. A* **2016**, *651*, 763–773. [CrossRef]
36. Miura, H.; Kobayashi, M.; Todaka, Y.; Watanabe, C.; Aoyagi, Y.; Sugiura, N.; Yoshinaga, N. Heterogeneous nanostructure developed in heavily cold-rolled stainless steels and the specific mechanical properties. *Scr. Mater.* **2017**, *133*, 33–36. [CrossRef]
37. Nakada, N.; Ito, H.; Matsuoka, Y.; Tsuchiyama, T.; Takaki, S. Deformation-induced martensitic transformation behavior in cold-rolled and cold-drawn type 316 stainless steels. *Acta Mater.* **2010**, *58*, 895–903. [CrossRef]
38. He, Y.; Godet, S.; Jonas, J.J. Observations of the Gibeon meteorite and the inverse Greninger–Troiano orientation relationship. *J. Appl. Crystallogr.* **2006**, *39*, 72–81. [CrossRef]
39. Landheer, H.; Offerman, S.E.; Petrov, R.H.; Kestens, L.A.I. The Role of α/γ Orientation Relationships during Ferrite Nucleation in an Fe-Cr-Ni Alloy. *Mater. Sci. Forum* **2007**, *558–559*, 1413–1418. [CrossRef]
40. Shakhova, I.; Dudko, V.; Belyakov, A.; Tsuzaki, K.; Kaibyshev, R. Effect of large strain cold rolling and subsequent annealing on microstructure and mechanical properties of an austenitic stainless steel. *Mater. Sci. Eng. A* **2012**, *545*, 176–186. [CrossRef]
41. Olson, G.; Cohen, M. Kinetics of nucleation strain-induced martensitic. *Met. Mater Trans. A* **1975**, *6*, 791–795. [CrossRef]
42. Odnobokova, M.; Belyakov, A.; Kaibyshev, R. Deformation microstructures and mechanical properties of an austenitic stainless steel subjected to warm rolling. *Mater. Sci. Forum* **2017**, *879*, 1414–1419. [CrossRef]
43. Mackenzie, J. Second paper on statistics associated with the random disorientation of cubes. *Biometrika* **1958**, *45*, 229–240. [CrossRef]
44. Kolmogorov, A.N. On the statistical theory of the crystallization of metals. *Bull. Acad. Sci. USSR Math. Ser.* **1937**, *1*, 355–359.
45. Johnson, W.A. Reaction kinetics in processes of nucleation and growth. *Am. Inst. Min. Met. Petro. Eng.* **1939**, *135*, 416–458.
46. Avrami, M. Kinetics of Phase Change. I General Theory. *J. Chem. Phys.* **1939**, *7*, 1103–1112. [CrossRef]
47. Starink, M.J. Dislocation versus grain boundary strengthening in SPD processed metals: Non-causal relation between grain size and strength of deformed polycrystals. *Mater. Sci. Eng. A* **2017**, *705*, 42–45. [CrossRef]
48. De Cooman, B.C.; Estrin, Y.; Kim, S.K. Twinning-induced plasticity (TWIP) steels. *Acta Mater.* **2018**, *142*, 283–362. [CrossRef]
49. Belyakov, A.; Sakai, T.; Miura, H. Fine-grained structure formation in austenitic stainless steel under multiple deformation at 0.5 Tm. *Mater. Trans. JIM* **2000**, *41*, 476–484. [CrossRef]
50. Hansen, N.; Huang, X.; Ueji, R.; Tsuji, N. Structure and strength after large strain deformation. *Mater. Sci. Eng. A* **2004**, *387*, 191–194. [CrossRef]
51. Khamsuk, S.; Park, N.; Gao, S.; Terada, D.; Adachi, H.; Tsuji, N. Mechanical properties of bulk ultrafine grained aluminum fabricated by torsion deformation at various temperatures and strain rates. *Mater. Trans.* **2014**, *55*, 106–113. [CrossRef]
52. Young, C.; Sherby, O. Sub-grain formation and sub-grain-boundary strengthening in Fe-based materials. *J. Iron Steel Inst.* **1973**, *211*, 640–647.

Publisher's Note: MDPI stays neutral with regard to jurisdictional claims in published maps and institutional affiliations.

© 2020 by the authors. Licensee MDPI, Basel, Switzerland. This article is an open access article distributed under the terms and conditions of the Creative Commons Attribution (CC BY) license (http://creativecommons.org/licenses/by/4.0/).